J Appl Physiol 108: 604–613, 2010.
First published December 24, 2009; doi:10.1152/japplphysiol.01157.2009.

Continuous estimates of dynamic cerebral autoregulation during transient hypocapnia and hypercapnia

N. E. Dineen,[1] F G. Brodie,[1] T. G. Robinson,[1] and R. B. Panerai[2]

[1]*Ageing and Stroke Medicine Group, Department of Cardiovascular Sciences, University of Leicester; and* [2]*Medical Physics Group, Department of Cardiovascular Sciences, University of Leicester, Leicester Royal Infirmary, Leicester, United Kingdom*

Submitted 9 October 2009; accepted in final form 21 December 2009

Dineen NE, Brodie FG, Robinson TG, Panerai RB. Continuous estimates of dynamic cerebral autoregulation during transient hypocapnia and hypercapnia. *J Appl Physiol* 108: 604–613, 2010. First published December 24, 2009; doi:10.1152/japplphysiol.01157.2009.—Dynamic cerebral autoregulation (CA) is the transient response of cerebral blood flow (CBF) to rapid blood pressure changes: it improves in hypocapnia and becomes impaired during hypercapnia. Batch-processing techniques have mostly been used to measure CA, providing a single estimate for an entire recording. A new approach to increase the temporal resolution of dynamic CA parameters was applied to transient hypercapnia and hypocapnia to describe the time-varying properties of dynamic CA during these conditions. Thirty healthy subjects (mean ± SD: 25 ± 6 yr, 9 men) were recruited. CBF velocity was recorded in both middle cerebral arteries (MCAs) with transcranial Doppler ultrasound. Arterial blood pressure (Finapres), end-tidal CO_2 (ET_{CO_2}; infrared capnograph), and a three-lead ECG were also measured at rest and during repeated breath hold and hyperventilation. A moving window autoregressive moving average model provided continuous values of the dynamic CA index [autoregulation index (ARI)] and unconstrained gain. Breath hold led to significant increase in ET_{CO_2} (+5.4 ± 6.1 mmHg), with concomitant increase in CBF velocity in both MCAs. Continuous dynamic CA parameters showed highly significant changes ($P < 0.001$), with a temporal pattern reflecting a delayed dynamic response of CA to changes in arterial P_{CO_2} and a maximal reduction in ARI of −5.1 ± 2.4 and −5.1 ± 2.3 for the right and left MCA, respectively. Hyperventilation led to a marked decrease in ET_{CO_2} (−7.2 ± 4.1 mmHg, $P < 0.001$). Unexpectedly, CA efficiency dropped significantly with the inception of the metronome-controlled hyperventilation, but, after ~30 s, the ARI increased gradually to show a maximum change of 5.7 ± 2.9 and 5.3 ± 3.0 for the right and left MCA, respectively ($P < 0.001$). These results confirm the potential of continuous estimates of dynamic CA to improve our understanding of human cerebrovascular physiology and represent a promising new approach to improve the sensitivity of clinical applications of dynamic CA modeling.

cerebral blood flow; end-tidal CO_2; autoregulation index; cerebrovascular reactivity

CEREBRAL BLOOD FLOW (CBF) is strongly influenced by arterial partial pressure of CO_2 (Pa_{CO_2}), which can also modulate the effectiveness of cerebral pressure autoregulation. The concept of cerebral autoregulation (CA), initially formulated by Lassen (17) to describe the tendency of CBF to remain relatively constant, despite changes in arterial blood pressure (BP), is now distinguished between static, as observed during steady-state conditions, or dynamic CA, which represents the response of CBF to transient changes in BP (1, 41).

Changes in Pa_{CO_2} have been shown to influence both static and dynamic CA. Hypocapnia reduces CBF and widens the plateau region of the static autoregulatory curve, representing improved CA, while also reducing the response time of CBF velocity (CBFV) following a sudden step change in BP (1, 34). On the other hand, hypercapnia causes an upward shift of the autoregulatory curve, impairing both static and dynamic CA (1, 28, 34).

CBF autoregulation and its dependence on Pa_{CO_2} have often been treated as separate mechanisms, leading to distinct methods of assessment in human subjects (24, 45). More recently, a number of studies have attempted to model their joint dynamic action and potential interactions, to advance understanding of human cerebral hemodynamics (2, 8, 21, 33, 35, 40, 42). The majority of these analyses, though, have not addressed transient changes in dynamic CA. In other words, parameters that are characteristically used to describe dynamic CA, such as the gain and phase of transfer function analysis (31, 46), or the autoregulation index (ARI) (41), were assumed to remain constant for relatively long periods of time, typically 5–10 min. We have investigated this important conceptual aspect of dynamic CA using a time-domain approach during transient changes in Pa_{CO_2} induced by either breath hold or hyperventilation. Previous studies have suggested that dynamic CA is likely to be a time-varying mechanism. However, with subjects breathing normally at rest, it has been difficult to determine how much of the variability of CA parameters could be ascribed to physiological influences, and how much was due to limitations in accuracy and precision of the mathematical techniques adopted to estimate CA parameters (11, 18, 21, 27, 29, 32, 38). Using the autoregressive-moving average (ARMA) technique, coupled to a relatively narrow moving-window segment of observation (MW-ARMA), we have addressed two main objectives: *1*) to confirm that time-varying dynamic CA parameters do indeed reflect physiological changes; and *2*) to describe how dynamic CA and other cerebral hemodynamic parameters respond to transient hypocapnia and hypercapnia in healthy human subjects.

METHODS

Subjects and measurements. Ethics approval was obtained from the Leicester, Northamptonshire, and Rutland Research ethics committee. Written, informed consent was obtained from 30 healthy participants between 20 and 39 yr old. Participants were excluded if they had a history of heart or vascular disease, hypertension, chronic obstructive pulmonary disease, migraine, epilepsy, renal failure, diabetes, or any neurological condition.

Address for reprint requests and other correspondence: R. B. Panerai, Dept. of Medical Physics, Leicester Royal Infirmary, Leicester LE1 5WW, UK (e-mail: rp9@le.ac.uk).

Participants were supine during recordings. Transcranial Doppler ultrasonography (Viasys Companion III) was used to measure CBFV as a measure of CBF. Bilateral insonation of the middle cerebral arteries (MCAs) was carried out using 2-MHz probes, held in place using a head frame. BP was measured noninvasively using finger arterial volume clamping (Finapres, Ohmeda 2300, Louisville, CO). A three-lead surface ECG was recorded continuously, and end-tidal CO_2 (ET_{CO_2}) was measured with an infrared capnograph (Capnocheck Plus) and nasal cannulae.

Each participant underwent an initial baseline recording of 5 min. A further four recordings of two breath-hold maneuvers and two hyperventilation maneuvers were repeated in random order with 5-min rest intervals between maneuvers. This provided 60 MCAs available for analysis of baseline recordings and 120 MCAs available for each type of maneuver. For the breath hold, participants were asked to hold their breath for as long as possible on normal inspiration. To standardize hyperventilation, participants were asked to breathe in sync with a metronome, producing a respiratory rate of 20 breaths/min for 90 s. Tidal volume was not controlled. A practice maneuver was performed before recording, and subjects were asked to breathe as deeply as possible in time with the metronome. Signals were digitized at 200 samples/s.

Data analysis. All data were visually inspected. The BP trace was calibrated, and linear interpolation was used to remove large spikes on the CBFV signal. A median filter of the appropriate width was used to remove small-amplitude noise on the CBFV trace. All channels were low-pass filtered at 20 Hz using a zero-phase Butterworth filter with a cutoff at 20 Hz. Each cardiac cycle was automatically marked from the ECG, and the mean BP, mean CBFV, and R-R interval were calculated for each cycle. The ET_{CO_2} value corresponding to each cardiac cycle was extracted by linear interpolation. The critical closing pressure (CrCP) and resistance-area product were estimated using the first harmonic of BP and CBFV of each cardiac cycle, as described previously (25). All signals were interpolated with spline polynomials and resampled at 5 Hz to obtain a uniform time base.

An ARMA (APPENDIX) structure was used to model the dynamic relationship between BP and CBFV for a given segment of data, leading to estimates of the dynamic ARI, as well as the unconstrained gain parameter of the model of Tiecks and Aaslid (4, 41). In their original communication, Tiecks et al. (41) constrained the three main parameters of their second-order model, gain (K), damping ratio (D), and time constant (*T*) to a set of 10 fixed values, with each combination corresponding to a value of ARI, ranging from 0 (no autoregulation) to 9 (best autoregulation). The "unconstrained" gain corresponds to the same parameter K, but, in this case, it can assume any real positive value (4). The advantages of investigating this additional parameter, represented as K′, will be discussed later. To obtain time-varying estimates of ARI and K′, the sampling rate was reduced to 0.6-s time intervals, and each calculation was performed for a 60-s segment of data. New estimates of ARI and K′ were obtained by shifting the 60-s window along the BP and CBFV signals every 0.6 s. For estimation of ARI, CBFV template response curves (41) were fitted to the first 6 s of the CBFV step response, corresponding to $N_{fit} = 10$ (APPENDIX). Time-varying estimates are expressed as ARI(*t*) and K′(*t*).

The main inflection points in the ET_{CO_2}, CBFV, ARI(*t*), and K′(*t*) signals were marked under visual inspection. For breath hold, the beginning of the ET_{CO_2} change was assumed as the point where the ET_{CO_2} signal disappeared. Likewise, the end of the maneuver was indicated by the return of the ET_{CO_2} signal. For hyperventilation, the beginning and end of the ET_{CO_2} change were taken as the instants of time corresponding to the inflection points of the downward plateau (Fig. 1). For CBFV, ARI(*t*), and K′(*t*), the time marks were placed at the first point where these variables started to change, at the beginning and end of the maneuver. These time marks were used to calculate the duration of the ET_{CO_2} change, as well as the time delay between the ET_{CO_2} change and the corresponding change in CBFV, ARI(*t*), or K′(*t*), both at the onset and at the outset of the maneuver.

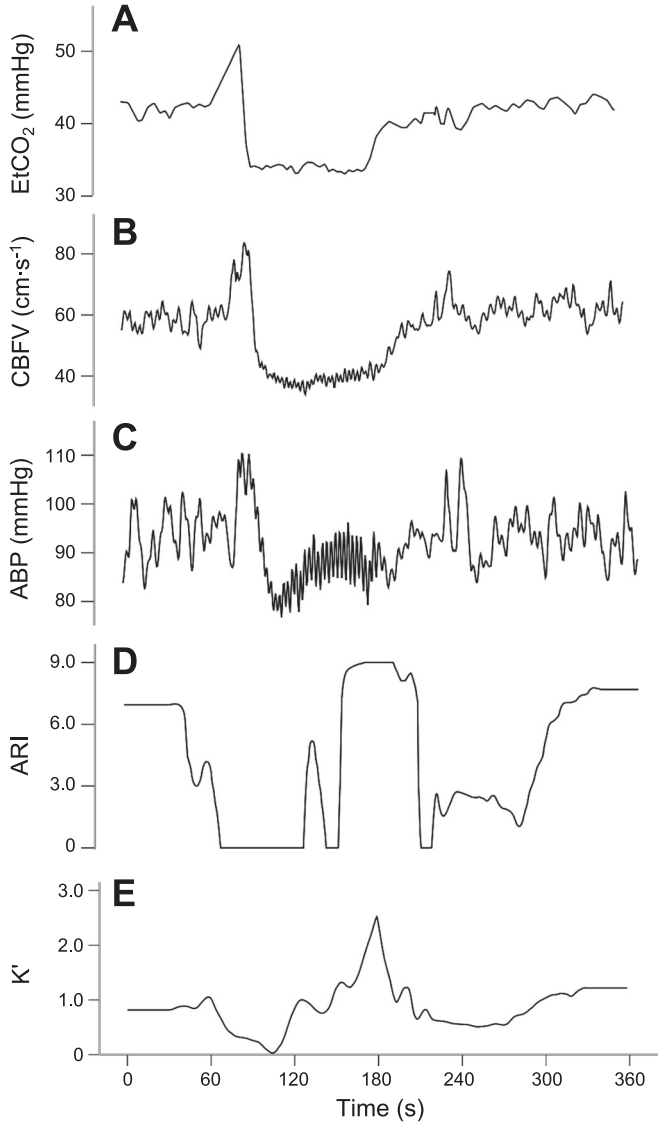

Fig. 1. Representative patterns of end-tidal CO_2 (ET_{CO_2}; *A*), cerebral blood flow velocity (CBFV; *B*), blood pressure (BP; *C*), autoregulation index time-varying estimate [ARI(*t*); *D*], and unconstrained gain time-varying estimate [K′(*t*); *E*] during hyperventilation in a 22-yr-old subject.

Statistics. Normally distributed data are expressed as means ± SD. Categorical participant demographics were compared using a χ^2 test.

To test the hypothesis that changes in ARI(*t*) and K′(*t*) were due to changes in Pa_{CO_2}, rather than due to random spontaneous fluctuations, maximum changes in the parameters during transient hypercapnia or hypocapnia were compared with corresponding maximum changes during baseline recordings. Maximum changes were calculated as the difference between absolute maximum values minus the mean value of the entire baseline recording, or the mean value of the 2-min segment of data preceding the respiratory maneuvers, respectively. Separate analyses were performed for the right and left MCA. Differences were tested using the paired Student's *t*-test.

To describe the transient response of ARI(*t*), K′(*t*), and other cerebral hemodynamic parameters following transient changes in Pa_{CO_2}, population coherent averages were calculated for a 180-s window of data, using the peak CBFV value recorded during the respiratory maneuver as the point of synchronism. The peak CBFV was chosen as the most reliable fiducial point for coherent averaging following visual inspection of individual recordings. Peak CBFV

always occurred at the end of the maneuver for breath hold and just before the beginning of hyperventilation. For this reason, the point of synchronism was placed at 45 s inside the 180-s window for hyperventilation and at 120 s for breath hold, respectively. Differences between coherent averages were tested with Student's *t*-test. A value of $P < 0.05$ was adopted to represent statistical significance.

RESULTS

Thirty healthy subjects (9 men), mean ± SD, age 25 ± 6 yr old were studied. None were current or ex-smokers. Other demographic and hemodynamic parameters are given in Table 1. Good quality recordings were obtained in all subjects for both right and left MCA. Clear changes in ARI(t) and K′(t) were confirmed by visual inspection in the large majority of recordings during breath hold or hyperventilation.

Representative changes in BP, CBFV, ET_{CO_2}, ARI(t), and K′(t) during hyperventilation are presented in Fig. 1 for an individual subject. CBFV showed a marked reduction a few seconds after the initial drop in ET_{CO_2}. BP also dropped by ~10 mmHg. Both ARI(t) and K′(t) fell at the beginning of the maneuver, but then rose markedly to achieve values above the preceding baseline period. Figure 2 illustrates corresponding changes in the same variables during breath hold in another subject. The CBFV change shows a clear delay in relation to the ET_{CO_2} signal, with both ARI(t) and K′(t) presenting marked reductions during hypercapnia. Fluctuations in ARI(t) and K′(t) were also observed during baseline, as exemplified by Fig. 3.

Figure 4 presents the mean ± SD maximum changes in ET_{CO_2}, CBFV, ARI(t), and K′(t) for both maneuvers for the right and left MCAs. Highly significant differences were confirmed for CBFV, ARI(t), K′(t), and ET_{CO_2} compared with corresponding changes during baseline (Table 2).

Figures 5 and 6 show the coherent averages produced for breath hold and hyperventilation, and Table 3 presents time delays between ET_{CO_2}, CBFV, and the dynamic CA parameters at the beginning and end of these maneuvers for the right MCA. Very similar values were obtained for the left MCA. Overall, there was an outstanding agreement between averages for the right and left MCA. Any differences between the two hemispheres were not significant. With the exception of heart rate, most variables and parameters showed opposite changes during breath hold and hyperventilation. During hypercapnia, CBFV started to rise 13.1 ± 6.5 s after the beginning of breath hold, which lasted 35.1 ± 16.4 s, leading to a sharp rise in CBFV near the end of the maneuver (Fig. 5*A*). On the other hand, during hypocapnia, CBFV started to fall 7.4 ± 3.0 s after the onset of hyperventilation and showed a long-lasting reduction for the duration of the maneuver (91.3 ± 4.3 s, Fig. 6, *A* and *B*). In both maneuvers, BP showed a similar directional change as CBFV, but of relatively small amplitude. The drop in ET_{CO_2} during hyperventilation (Fig. 6*B*) was consistent with expectations, but the expected increase in Pa_{CO_2} during breath hold was not detected by ET_{CO_2} until the end of the maneuver (Fig. 5*B*), due to the lack of expired gas, as it will be discussed later. Although the changes observed in CrCP and resistance-area product were relatively small (Figs. 5, *G* and *H*, and 6, *G* and *H*), their consistent directional changes can help to explain the overall change in CBFV. The time courses of ARI(t) and K′(t) were not exactly the same. During breath hold, ARI(t) started to fall before the rise in CBFV, 12.0 ± 11.0 s after the initial change in ET_{CO_2} (Fig. 5*C*). Its return to baseline values

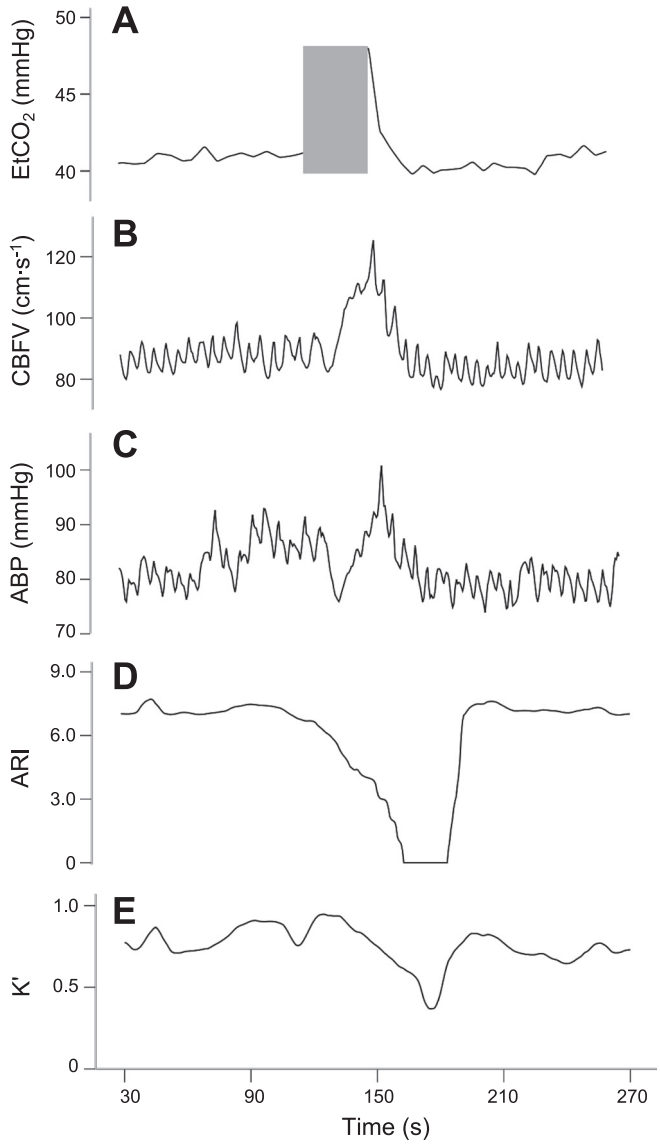

Fig. 2. Representative patterns of ET_{CO_2} (*A*), CBFV (*B*), BP (*C*), ARI(t) (*D*), and K′(t) (*E*) during breath hold in a 22-yr-old subject. The shaded area indicates the lack of ET_{CO_2} signal during breath hold.

Table 1. *Volunteer demographic and baseline parameters*

						Smokers	
Male-Female	Systolic BP, mmHg	Diastolic BP, mmHg	Heart Rate, beats/min	Respiratory Rate, min^{-1}	Body Mass Index, kg/m^2	Current	Ex
9:21	120 ± 14 (96–138)	75 ± 9 (62–92)	68 ± 11 (52–90)	14 ± 4 (6–22)	22 ± 3 (17–29)	0	0

Values are means ± SD (range). BP, blood pressure.

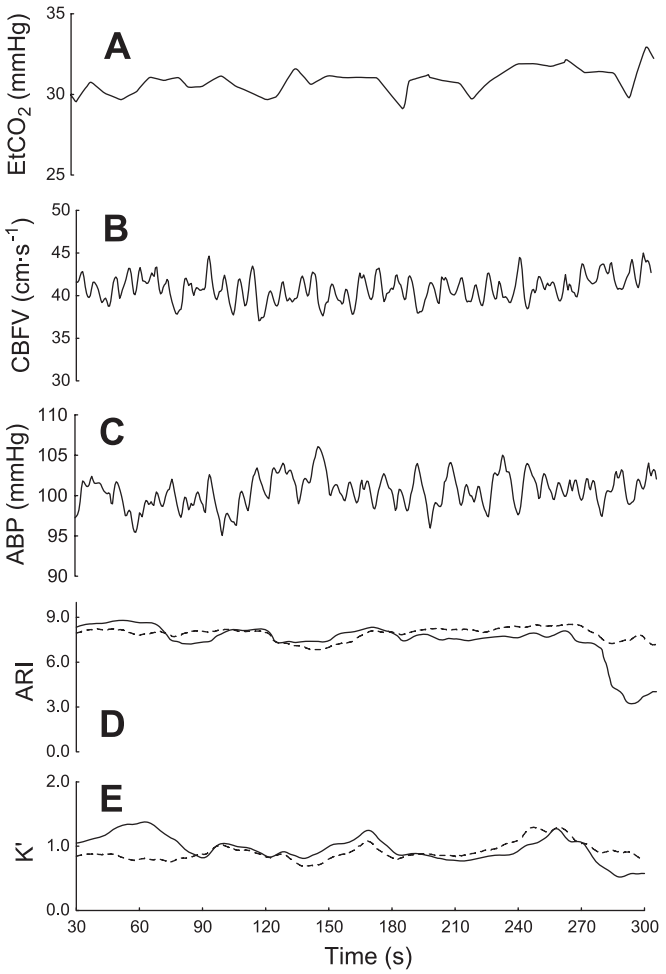

Fig. 3. Representative fluctuations in ET_{CO_2} (*A*), right middle cerebral artery (MCA) CBFV (*B*), BP (*C*), ARI(*t*) (*D*), and K′(*t*) (*E*) during baseline. ARI and K′(*t*) are for right (solid line) and left (dashed line) MCA. With the exception of CBFV, the maximum changes in the other parameters compare well with the mean values given in Table 2.

only started when CBFV had already returned to its original value, 30.0 ± 10.2 s after ET_{CO_2} reached its peak. K′(*t*) did not show the same initial drop before CBFV as ARI(*t*) did, and it also decreased more slowly, but their minima occurred approximately at the same point in time (Fig. 5, *C* and *D*). In both cases, there was a considerable delay between the peak of mean ET_{CO_2} and their minimum value (Table 3). During hyperventilation, the main feature of the ARI(*t*) and K′(*t*) averages was the initial fall, followed by a steep recovery (Fig. 6, *C* and *D*). This pattern was also confirmed in most individual recordings (Fig. 1), suggesting that it was not an artifact of the averaging process. Again, at the beginning of the maneuver, ARI(*t*), and in this case also K′(*t*), started to drop before any changes in CBFV became evident (Fig. 6*A*). On the other hand, both ARI(*t*) and K′(*t*) started to return to their baseline values shortly after CBFV did, and with time delays of 17.3 ± 21.9 s (ARI) and 16.3 ± 24.5 s (K′) in relation to the turning point of ET_{CO_2} at the end of the maneuver (Fig. 6*B*). Despite these similar times of inflection, there was a clear difference between the ARI(*t*) and K′(*t*) temporal patterns, with the former achieving its peak value earlier in the maneuver, while the latter rose to a plateau and then showed a secondary peak near the end of hyperventilation (Fig. 6, *C* and *D*). These patterns will be discussed further below.

DISCUSSION

Main findings. To our knowledge, this is the first study to demonstrate that short-term transient changes in dynamic CA parameters represent true physiological phenomena, rather than artifacts due to estimation technique. This finding should open many opportunities for investigating the physiology of CA under diverse physiological scenarios (e.g., tilting, exercise, cognitive stimulation), where measurement conditions are not stationary, and during special interventions that could allow greater insight into the different mechanisms involved in the regulation of CBF in humans. Time-varying blood flow autoregulation was reported in the kidney (47), and it has also been suggested as a possibility in the cerebral circulation (11, 18, 20, 27, 29, 32, 38). The demonstration that the MW-ARMA method provides time-varying estimates of ARI(*t*) and K′(*t*), in agreement with the well-known effects of hyper- and hypocapnia on dynamic CA (1, 7, 28), can be regarded as a key step toward the incorporation of the time-varying approach in physiological and clinical studies of human CA.

One clear example of the potential advantages of the time-varying approach was the unexpected finding that dynamic autoregulation is temporarily depressed at the early stages of hyperventilation (Fig. 6, *C* and *D*). The consistency of this initial dip across the population suggests a physiological origin. We can only speculate that this might be a stress-related response to the mental effort to synchronize breathing to the metronome, and that the depression in CA could be the result of competing demands for increased CBF to meet additional metabolic supply. Previous studies have shown that the immediate reaction to cognitive stimulation induces rapid rises in BP and CBFV, as depicted in Fig. 6, *A* and *E* (22). Moreover, depression of dynamic CA was also reported in similar conditions involving metabolic stimulation (23, 30). By performing dedicated experiments, it should be possible to obtain the separate components of ARI(*t*) and K′(*t*), due to the stress-related response and the subsequent recovery of dynamic CA due to hypocapnia. If these studies confirm the transient effects of stressors on dynamic CA, they could shed light on many relevant physiological and clinical phenomena, such as the sequence of events leading to syncope in otherwise healthy subjects. Classical methods of dynamic CA assessment have consistently failed to demonstrate involvement of CA as a determinant of syncope, but these techniques had to rely on recordings lasting from 3 to 5 min, during which a transient depression in CA would be missed. However, if stressors can induce short-term depression in CA, lasting up to 30 s or eventually more, then it is possible that this could explain the occurrence of syncope in situations in which other determinants cannot be identified (26, 43).

An additional contribution of this study was the inclusion of unconstrained gain, as a new parameter to express relative changes in dynamic CA efficiency, compared with the more classical index of dynamic CA expressed by the ARI (4, 41). The expectation that K′(*t*) would show a better coefficient of variation than the ARI(*t*) was not confirmed by the coherent averages and corresponding sample-by-sample standard errors in Figs. 5 and 6. On the other hand, the difference in temporal

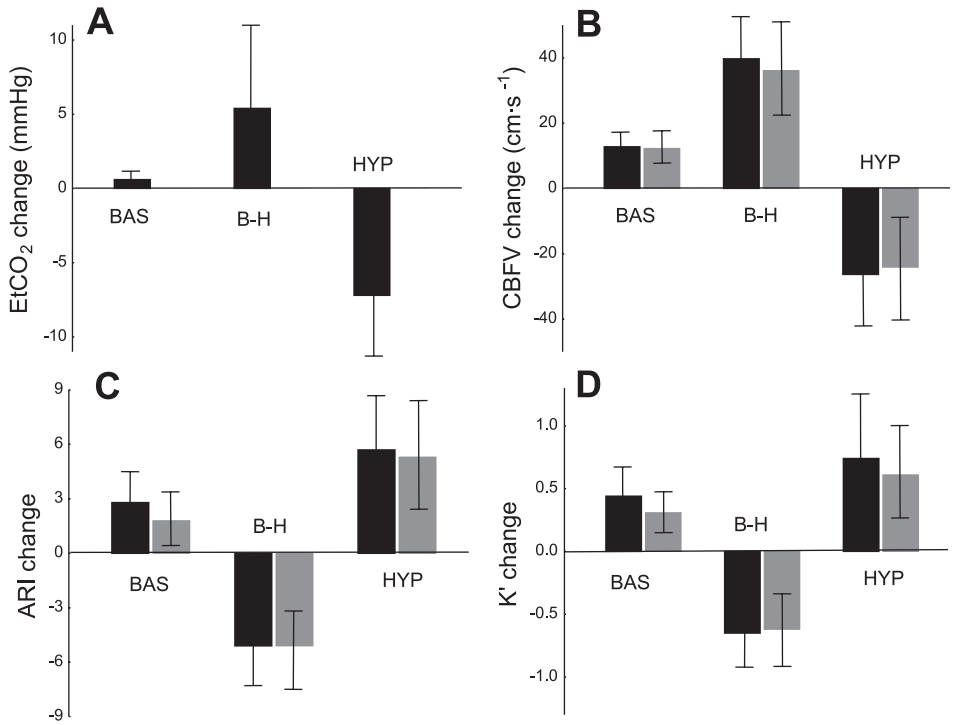

Fig. 4. Maximum change in ET_{CO_2} (*A*), CBFV (*B*), ARI(*t*) (*C*), and K′(*t*) (*D*) during breath hold (B-H) and hyperventilation (HYP) maneuvers compared with corresponding values during baseline (BAS) for the right (solid bars) and left (shaded bars) MCA. Values are means ± SD.

patterns between K′(*t*) and ARI(*t*) in response to both hyper- and hypocapnia are of interest and deserve further attention, as they could indicate greater sensitivity of K′(*t*) compared with ARI(*t*). Two aspects of K′*t*) seem to point in this direction. During breath hold, the gradual decrease in K′(*t*), compared with ARI(*t*) (Fig. 5, *C* and *D*), suggest that the former might have a better association with Pa_{CO_2}, as reflected by the gradual increase in CBFV (Fig. 5*A*), than ARI(*t*), which shows a much more pronounced change, possibly due to its tendency to drop to zero at low values of ARI, as illustrated in Figs. 1 and 2 and reported previously (29, 32). During hyperventilation, the pattern for K′(*t*) (Fig. 6*D*) also shows better correlation with the ET_{CO_2} change, although the final peak would suggest a disproportional nonlinear response. Finally, one practical advantage of K′ compared with ARI is the more straighforward calculation directly from the ARMA parameters (APPENDIX), thus abbreviating the need to estimate CBFV step responses and fit the Tiecks et al. (41) template curves for estimation of ARI.

Time-varying properties of CBF regulation mechanisms. From a conceptual standpoint, the complex and multivariate nature of CBF regulatory mechanisms would indicate that temporal variability of parameters describing the dynamic relationship between BP and CBFV should be the norm, rather than the exception. This perspective is supported by different lines of investigation into spontaneous cerebral metabolic fluctuations (5, 9, 13, 15, 44) or looking into the temporal and spatial heterogeneity of brain microcirculation (12, 14, 16). During observations at rest, temporal variability in CBF regulatory mechanisms are likely to be dominated by random effects, but also showing deterministic contributions from covariates, such as fluctuations in Pa_{CO_2} or mental activation. Accurate analysis of these phenomena in humans is made difficult by limitations of the tools available for modeling dynamic autoregulation based on noninvasive recordings. Reproducibility studies suggest that at least 45 subjects are needed to detect a change in ΔARI = 1 unit with a statistical

Table 2. *Maximum relative changes in parameter values during baseline recordings and respiratory maneuvers*

		Breath Hold		Hyperventilation	
	Baseline, Maximum Changes	Maximum changes	*P* value*	Maximum changes	*P* value*
CBFV, cm/s					
Right	12.8 ± 4.7	39.7 ± 14.2	<0.001	26.3 ± 15.8	<0.001
Left	12.3 ± 5.1	36.1 ± 14.4	<0.001	24.1 ± 16.6	<0.001
ARI(*t*)					
Right	2.8 ± 1.7	5.1 ± 2.4	<0.001	5.7 ± 2.9	<0.001
Left	1.8 ± 1.6	5.1 ± 2.3	<0.001	5.3 ± 3.0	<0.001
K′(*t*)					
Right	0.44 ± 0.25	0.65 ± 0.28	<0.001	0.74 ± 0.55	0.0002
Left	0.31 ± 0.17	0.62 ± 0.32	<0.001	0.61 ± 0.38	<0.001
ET_{CO_2}, mmHg	0.6 ± 0.5	5.4 ± 6.1	<0.001	7.2 ± 4.1	<0.001

Values are means ± SD. CBFV, cerebral blood flow velocity; ARI(*t*), autoregulation index time-varying estimate; K′(*t*), unconstrained gain time-varying estimate; ET_{CO_2}, end-tidal CO_2. Right and left refer to middle cerebral artery. *Difference between each maneuver vs. corresponding values for baseline recording.

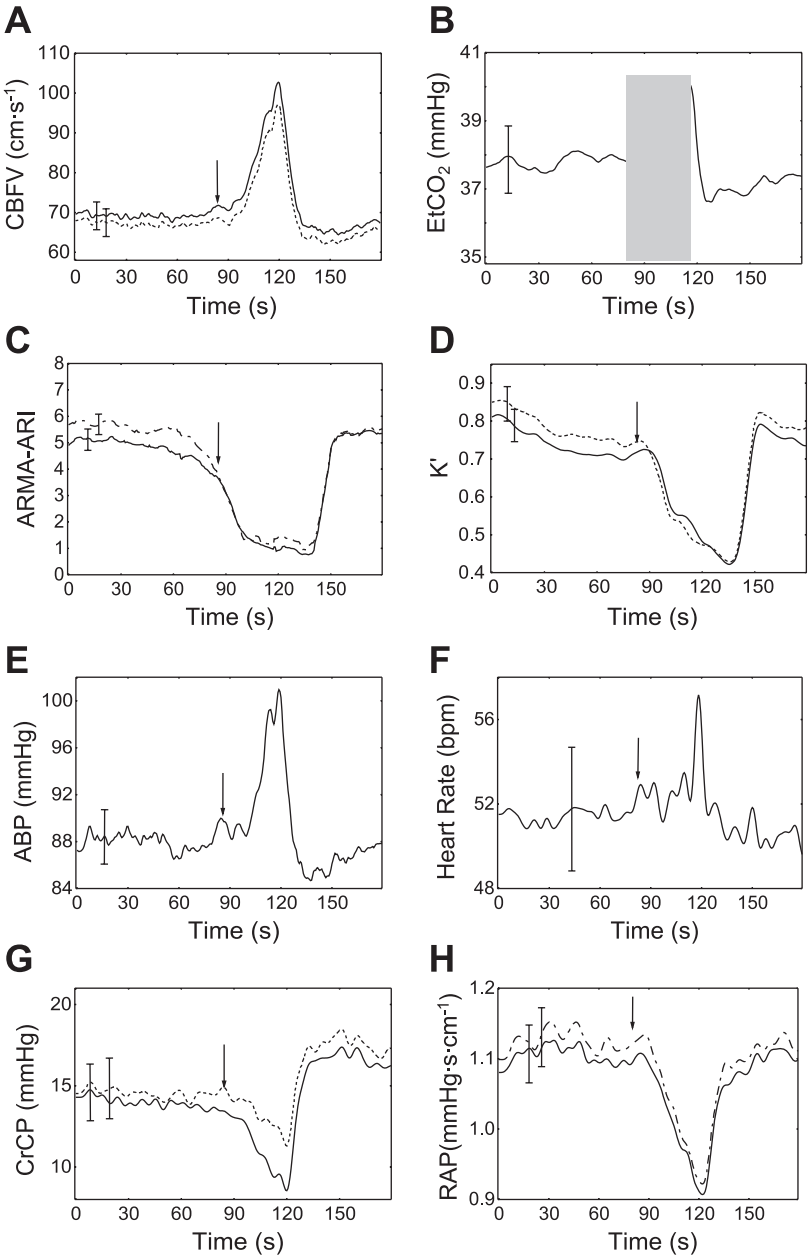

Fig. 5. Population coherent averages of breath-hold recordings. CBFV (*A*), ET_{CO_2} (*B*), ARI (*C*), K′ (*D*), BP (*E*), and heart rate (*F*) are plotted against time. *G*: critical closing pressure (CrCP). *H*: resistance-area product (RAP). The arrow indicates start of maneuver. In *A*, *C*, *D*, *G*, and *H*, the solid line represents right MCA, and dashed line represents left MCA. The shaded area indicates the lack of ET_{CO_2} signal during breath hold. The maximum SE bar is shown for each plot. ARMA, autoregressive moving average; bpm, beats/min.

power of 80% at $P = 0.05$ or, alternatively, 11 subjects to detect a change of $\Delta ARI = 2$ (3). Given that the present study enrolled 30 subjects, the maximum changes in ARI detected during baseline are likely to be significant (Table 2), but the much larger changes observed as the result of hyper- and hypocapnia are certainly very meaningful. This demonstration suggests that the MW-ARMA technique could also be suitable to study spontaneous fluctuations in dynamic CA at rest, but further research is undoubtedly needed. Hitherto, the dynamic influences of Pa_{CO_2} on the cerebral circulation have been described by the relationship between ET_{CO_2} and CBFV. Using accurate step changes in ET_{CO_2}, Poulin and coworkers (36, 37) have shown that the CBFV dynamic response to both hypercapnia and hypocapnia can be described by first-order models containing pure time delays. For hypocapnia, a more complex model involving both fast and slow components was required. A mean ± SD pure time delay of 6.0 ± 0.07 s was reported for hypercapnia, and the first-order time constants were 45.3 ± 13.4 and 6.1 ± 0.5 s for the onset and offset changes, respectively (36). Direct comparison with our results is not straightforward, since we have used voluntary breath hold rather than the more controllable dynamic end-tidal forcing adopted by Poulin et al. (36). Those authors also used much longer maneuvers, lasting 20 min, instead of the relatively short breath holds that lasted 35 s, on average, in our case. Despite these differences, the time delays between ET_{CO_2} and CBFV listed in Table 3 are in good qualitative agreement, showing a much slower response of CBFV at the onset of the maneuver than in the return to normocapnia. For hypocapnia, the slow component proposed by Poulin et al. (37) could be ignored for our purposes, given the relatively short duration of the hyperventilation maneuvers compared with the 20 min of end-tidal

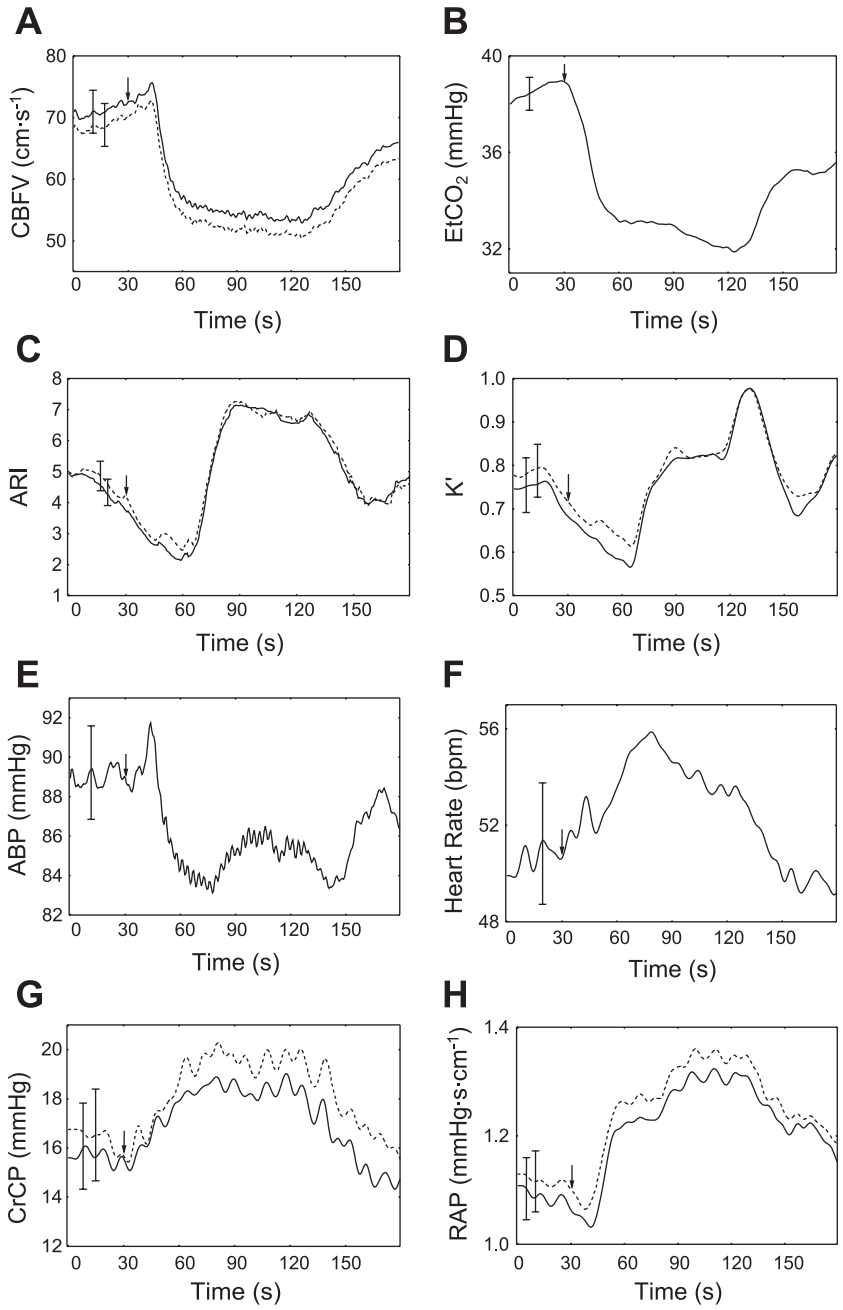

Fig. 6. Population coherent averages of hyperventilation recordings. CBFV (*A*), ET_{CO_2} (*B*), ARI (*C*), K′ (*D*), BP (*E*), and heart rate (*F*) are plotted against time. *G*: CrCP. *H*: RAP. Arrow indicates start of maneuver. In *A*, *C*, *D*, *G*, and *H*, the solid line represents right MCA, and dashed line represents left MCA. The maximum SE bar is shown for each plot.

forcing adopted by those investigators. For the fast component, the mean pure time delay was 3.9 ± 1.7 s, with an onset time constant of 6.6 ± 4.7 s and an off response time constant of 14.3 ± 12.9 s. Again, there was good qualitative agreement with our results (Table 3), showing that, for hypocapnia, the onset of the CBFV response to the ET_{CO_2} change was slower than in the return to baseline. From the temporal patterns shown in Figs. 5 and 6 and the time delays in Table 3, it can be observed that ARI(t) and K′(t) do not follow the same temporal dependence in relation to ET_{CO_2} as CBFV does. During breath hold, K′(t) started to respond to the ET_{CO_2} change earlier than CBFV ($P < 0.015$), but, for ARI(t), this difference was not significant. On the other hand, during the return to normocapnia, the autoregulatory response is much slower than that of CBFV ($P < 10^{-5}$). These observations suggest that changes in autoregulation in response to hypercapnia have the inverse behavior of CBFV, showing a faster response to the onset phase than in the return to normocapnia ($P < 10^{-5}$). Similar comparisons during hypocapnia are hindered by the occurrence of the autoregulation "dips" at the onset of hyperventilation, as discussed above. Nevertheless, as soon as ARI(t) and K′(t) recover from the initial depression, their rate of rise is faster than during the return to normocapnia (Fig. 6, *C* and *D*). The time delays in Table 3 also indicate that the return from hypocapnia to normocapnia starts to occur much earlier than in the case of hypercapnia for ARI(t) ($P < 0.006$), but with a slower rate of change when Fig. 5, *C* and *D*, are compared with Fig. 6, *C* and *D*. These observations lead to the hypothesis that the mechanisms influencing changes in autoregulation are likely to present directional sensitivity,

Table 3. *Time intervals for changes in CBFV (right middle cerebral artery) and time-varying dynamic cerebral autoregulation parameters following transient changes in ET_{CO_2} induced by respiratory maneuvers*

	Breath Hold		Hyperventilation	
Time Interval	Onset	Return to baseline	Onset	Return to baseline
Duration of ET_{CO_2} change	35.1 ± 16.4		91.3 ± 4.3	
ET_{CO_2}-CBFV	13.1 ± 6.5	2.8 ± 2.6	7.4 ± 3.9	9.1 ± 7.3
ET_{CO_2}-ARI(t)	12.0 ± 11.0	30.0 ± 10.2	31.0 ± 7.6	17.3 ± 21.9
ET_{CO_2}-K′(t)	8.6 ± 11.2	18.7 ± 9.9	28.5 ± 10.1	16.3 ± 24.5

Values are means ± SD in seconds.

which would explain their asymmetric behavior in relation to changes from normocapnia to either hypo- or hypercapnia and vice versa. Future work in this area should take into account some of the limitations to be addressed below.

Study limitations. Transcranial Doppler ultrasound can provide reliable estimates of CBF, as long as the diameter of the MCA remains relatively constant. This is a particular concern in this study because of the significant changes in Pa_{CO_2} induced by the respiratory maneuvers, and the time-varying estimates of dynamic CA parameters. Previous studies of MCA diameter changes in the presence of relatively large changes in Pa_{CO_2} concluded that significant changes in diameter are not likely to occur (10, 39). Nevertheless, it is important to keep in mind that, if changes in MCA diameter were taking place during the maneuvers, they could distort the temporal patterns of ARI(t) and K′(t) shown in Figs. 1–3, 5, and 6.

Allowing subjects to control their own breath hold and hyperventilation maneuvers inherently leads to greater intersubject variability, compared with more controlled protocols based on dynamic end-tidal forcing, for example (36, 37). Future studies adopting the latter are likely to provide additional useful information, but our choice of a simpler approach was greatly influenced by the intention to translate this research to clinical applications. Nevertheless, the choice of using breath hold to induce hypercapnia presents the additional limitation of precluding measurement of ET_{CO_2} during most of the maneuver, and this is one aspect of the protocol that should be reviewed in future studies. Due to the lack of ET_{CO_2} signal, the time intervals presented in Table 3 were derived from the effective start of breath hold, when the ET_{CO_2} disappeared, to the moment the signal was present again, corresponding to the effective end of the maneuver. These estimates do not reflect the additional time it takes for ET_{CO_2} to change following the beginning and end of the maneuver and are thus different from the approach adopted to detect equivalent times for the hyperventilation maneuver. For this reason, the time delays for hypercapnia (Table 3) should be interpreted with caution. Despite this limitation, the ET_{CO_2} values at the end of breath hold allowed confirmation of the marked hypercapnia achieved, and its gradual built up was reflected in the time course of CBFV (Fig. 5*A*).

The duration of the moving window of the MW-ARMA technique, selected as 60 s in our case, can be seen as a limitation of the best temporal resolution that can be achieved with this approach. Tests performed with windows of 30 s (results not shown) have provided similar patterns of ARI(t) and K′(t) to the standard 60-s window results shown in Figs. 5 and 6, but with better temporal resolution, despite greater individual variability. The temporal relationship between the dynamic CA parameter estimates and the moving-window position also has implications for the interpretation of results. For any given 60-s segment of data being modeled, the corresponding estimates of ARI(t) and K′(t) can be assumed to be at the beginning, middle, or end of the moving window. Whatever the choice though, it is important to stress that the resulting estimates will be the same, but will obviously be shifted in time in relation to the original values of BP and CBFV. The decision to place model estimates at the center of the moving window had the objective of keeping a "zero-phase" difference with the continuous BP and CBFV signals. Had the choice been to place estimates at the end of the window, those would be delayed compared with the original data, making the interpretation of the time intervals given in Table 3 more difficult. It could be argued that placing estimates in the middle of the window involves the use of 30 s of "future" data, but, as mentioned above, the temporal patterns of ARI(t) and K′(t) are exactly the same in both cases. Moreover, the use of 30 s of "past" data and 30 s of "future data" is part of the temporal resolution limitation alluded to above, behaving in similar fashion to low-pass moving averaging filters ("boxcar filters") that use both past and future data to maintain a zero phase. Finally, the choice of placing estimates in the middle of the moving window also balances evenly the loss of data corresponding to the first and last 30 s of data, for which estimates of ARI(t) and K′(t) cannot be extracted. In our case, this was not a problem, since each maneuver was preceded or followed by at least 2 min of baseline data.

Previous studies of the influence of Pa_{CO_2} on CBF have adopted multivariate models to take into account potential interactions between Pa_{CO_2} and BP (6, 20, 21, 33, 35). Ideally, more comprehensive models with the potential to incorporate nonlinear effects, like the ones proposed by Mitsis et al. (20, 21), should be extended to provide similar temporal resolution as the MW-ARMA that we have adopted. The lack of multivariate modeling in our case though is unlikely to have had a marked influenced on the ARI(t) and K′(t) results for two main reasons. First, as demonstrated previously, separate analysis of the influences of BP and Pa_{CO_2} on CBFV is acceptable due to the different frequency bands in which they operate (33). If the slow changes in CBFV and ABP observed in Figs. 1, 5, and 6 are removed by high-pass filtering with cutoff frequencies in the range 0.005–0.007 Hz, the resulting patterns of ARI(t) and K′(t) are approximately the same (results now shown). In other words, the ARI(t) and K′(t) patterns are not the result of the slow changes in CBFV caused by transient hyper- or hypocapnia, but due to the changing nature of the BP-CBFV dynamic relationship, which operates at higher frequencies. This conclusion is supported by the detailed analysis of the ARI(t) and K′(t) temporal patterns described above and the distinct time

delays involved. Second, it is well known that Pa_{CO_2} also influences BP, but this is more relevant in the analysis of the Pa_{CO_2}-CBFV relationship than in our case, since any influences of Pa_{CO_2} on BP, albeit relatively small (Figs. 5*E* and 6*E*), were automatically incorporated in the BP-CBFV dynamic relationship, which we analyzed.

In summary, a new approach, combining a moving data window with time-domain ARMA modeling, allowed calculation of dynamic CA parameters with much higher temporal resolution than the classical "batch" processing of recordings lasting several minutes. In addition to the dynamic CA index (ARI), a new parameter, namely the unconstrained gain of CA (K′), was also studied with this method during maneuvers intended to induce changes in Pa_{CO_2}. Both parameters showed time-varying properties in response to hypercapnia and hypocapnia, with temporal patterns suggesting new hypotheses about the influence of Pa_{CO_2} on human CBF regulation. Of particular interest was a temporary depression of both CA parameters at the early stages of hypocapnia, which could indicate their sensitivity to stress of cognitive origin. This new approach opens many avenues for investigating the physiology of dynamic CA in humans in nonstationary situations, like exercise, posture changes, and cognitive and/or sensorimotor stimulation. Future work should also explore the potential of this approach to improve the sensitivity of current techniques used for assessing patients with cerebrovascular conditions.

APPENDIX

ARMA Implementation of Tiecks Model

The model proposed by Tiecks et al. (41) uses a second-order differential equation to predict the velocity signal $V(t)$ corresponding to a pressure change given by $P(t)$. Initially, the pressure change is normalized as:

$$dP(t) = \frac{P(t)}{1 - CrCP} \tag{A.1}$$

where CrCP is a fraction of the baseline pressure. The relative velocity $[\hat{V}(t)]$ change estimated by the model is given by:

$$\hat{V}(t) = 1 + dP(t) - K \times x_2(t) \tag{A.2}$$

where K represents a gain parameter in the second-order equation, and $x_2(t)$ is a state variable obtained from the following state equation system representing a second-order linear differential equation:

$$x_1(t) = x_1(t-1) + \frac{dP(t-1) - x_2(t-1)}{f \times T} \tag{A.3}$$

$$x_2(t) = x_2(t-1) + \frac{x_1(t-1) - 2 \times D \times x_2(t-1)}{f \times T} \tag{A.4}$$

where f is the sampling frequency. In the original proposal of Tiecks et al. (41), only 10 combinations of the parameters K, D, and T were considered, according to the values given in their Table 3, which also shows the corresponding value of ARI for each combination of these parameters.

To obtain the transfer function between $P(t)$ and $V(t)$, *Eqs. A2–A4* can be written as their Z-transforms:

$$V(z) = P(z) - KX_2(z) \tag{A.5}$$

$$X_1(z) = z^{-1}X_1(z) + \frac{P(z) - z^{-1}X_2(z)}{T'} \tag{A.6}$$

$$X_2(z) = z^{-1}X_2(z) + \frac{X_1(z) - 2Dz^{-1}X_2(z)}{T'} \tag{A.7}$$

where $T' = f \cdot T$. Solving the above equations leads to the z-transfer function:

$$\frac{V(z)}{P(z)} = \frac{\left(1 - \frac{K}{T'}\right)^2 + z^{-1}\left(\frac{1}{T'^2} + \frac{2D}{T'} - 2\right) + z^{-2}\left(1 - \frac{2D}{T'}\right)}{1 + z^{-1}\left(\frac{1}{T'2} + \frac{2D}{T'} - 2\right) + z^{-2}\left(1 - \frac{2D}{T'}\right)} \tag{A.8}$$

A similar result was previously reported (19). *Eq. A8* can be written as:

$$\frac{V(z)}{P(z)} = \frac{a + bz^{-1} + cz^{-2}}{1 + bz^{-1} + cz^{-2}} \tag{A.9}$$

where

$$a = \left(1 - \frac{K}{T'}\right)^2 \tag{A.10}$$

$$b = \frac{1}{T'^2} + \frac{2D}{T'} - 2 \tag{A.11}$$

$$c = 1 - \frac{2D}{T'} \tag{A.12}$$

Applying the inverse Z-transform to *Eq. A9* results in:

$$v(n) = ap(n) + b\big[p(n-1) - v(n-1)\big] + c\big[p(n-2) - v(n-2)\big] \tag{A.13}$$

where $p(n)$ and $v(n)$ are discrete samples of $V(t)$ and $P(t)$, respectively.

Equation A13 has the structure of a particular ARMA model, where the past samples of both input and output are weighted by the same coefficients. Although dynamic autoregulation has been previously modeled with ARMA structures of order [2, 3] (19, 27, 32), the above derivation demonstrates that the strict representation of the model of Tiecks and Aaslid behaves more as an ARMA of order [2, 1].

Following the estimation of the ARMA coefficients in *Eq. A13*, *Eq. A10* can be used to obtain corresponding estimates of K′, which is the unconstrained gain parameter, able to assume values not limited to the original 10 values imposed by Tiecks et al. (41). Hence:

$$K' = \frac{1 - a}{1 + b + c} \tag{A.14}$$

With T'^2 replaced by summation of *Eqs. A11* and *A12*. In theory, $a \leq 1$ and $b + c \geq -1$. However, due to the possibility of estimation bias, it is necessary to add small residuals ε_1, ε_2 to *Eq. A14*:

$$K' = \frac{1 - a + \varepsilon_1}{1 + b + c + \varepsilon_2} \tag{A.15}$$

Typical values of ε_1 and ε_2 are 0.1.

For a given segment of data, ARMA coefficients (*Eq. A13*) are estimated by least squares, leading to corresponding estimates of K′ (*Eq. A15*). This approach is computationally more efficient than the original exhaustive search adopted by Chacon et al. (4).

Once the ARMA parameters have been calculated, the CBFV step response can be estimated from *Eq. A13*, and the ARI parameter can then be extracted by least squares fitting of the corresponding Tiecks et al. (41) model responses using the first N_{fit} samples of the ARMA step response.

DISCLOSURES

No conflicts of interest are declared by the author(s).

REFERENCES

1. **Aaslid R, Lindegaard KF, Sorteberg W, Nornes H.** Cerebral autoregulation dynamics in humans. *Stroke* 20: 45–52, 1989.
2. **Ainslie PN, Celi L, McGrattan K, Peebles K, Ogoh S.** Dynamic cerebral autoregulation and baroreflex sensitivity during modest and severe step changes in arterial pCO2. *Brain Res* 1230: 115–124, 2008.
3. **Brodie FG, Atkins ER, Robinson TG, Panerai RB.** Reliability of dynamic cerebral autoregulation measurements using spontaneous fluctuations in blood pressure. *Clin Sci* 116: 513–520, 2009.
4. **Chacon M, Nunez N, Henriquez C, Panerai RB.** Unconstrained parameter estimation for assessment of dynamic cerebral autoregulation. *Physiol Meas* 29: 1179–1193, 2008.
5. **Dora E, Kovach AGB.** Metabolic and vascular volume oscillations in the cat brain cortex. *Acta Physiol Acad Scient Hung* 57: 261–275, 1981.
6. **Dumville J, Panerai RB, Lennard NS, Naylor AR, Evans DH.** Can cerebrovascular reactivity be assessed without measuring blood pressure in patients with carotid artery disease? *Stroke* 29: 968–974, 1998.
7. **Edwards MR, Devitt DL, Hughson RL.** Two-breadth CO_2 test detects altered dynamic cerebrovascular autoregulation and CO_2 responsiveness with changes in arterial P_{CO_2}. *Am J Physiol Regul Integr Comp Physiol* 287: R627–R632, 2004.
8. **Edwards MR, Lin DC, Hughson RL.** Modeling the interaction between perfusion pressure and CO_2 on cerebral blood flow. *Adv Exp Med Biol* 499: 285–290, 2001.
9. **Fox MD, Raichle ME.** Spontaneous fluctuations in brain activity observed with functional magnetic resonance imaging. *Nat Rev Neurosci* 8: 700–711, 2007.
10. **Giller CA, Bowman G, Dyer H, Mootz L, Krippner W.** Cerebral arterial diameters during changes in blood pressure and carbon dioxide during craniotomy. *Neurosurgery* 32: 737–742, 1993.
11. **Giller CA, Mueller M.** Linearity and non-linearity in cerebral hemodynamics. *Med Eng Phys* 25: 633–646, 2003.
12. **Gotoh F, Fukuuchi Y, Okayasu H, Tanaka K, Suzuki N, Kobari M.** Rhythmic changes in diameter of pial vessels and function of autonomic nervous system. In: *Cerebral Blood Flow: Effects of Nerves and Neurotransmitters*, edited by Heistad DD. Amsterdam: Elsevier North Holland, 1982, p. 409–417.
13. **Halsey JHJ, McFarland S.** Oxygen cycles and metabolic autoregulation. *Stroke* 5: 219–225, 1974.
14. **Hudetz AG.** Blood flow in the cerebral capillary network: a review emphasizing observations with intravital microscopy. *Microcirculation* 4: 233–252, 1997.
15. **Jones SC, Williams JL, Shea M, Easley KA, Wei D.** Cortical cerebral blood flow cycling: anesthesia and arterial pressure. *Am J Physiol Heart Circ Physiol* 268: H569–H575, 1995.
16. **Kuga N, Hirata T, Sakai I, Tanikawa Y, Chiou HY, Kitanishi T, Matsuki N, Ikegaya Y.** Rapid and local autoregulation of cerebrovascular blood flow: a deep-brain imaging study in the mouse. *J Physiol* 587.4: 745–752, 2009.
17. **Lassen NA.** Cerebral blood flow and oxygen consumption in man. *Physiol Rev* 39: 183–238, 1959.
18. **Latka M, Turalska M, Glaubic-Latka M, Kolodziej W, Latka D, West BJ.** Phase dynamics in cerebral autoregulation. *Am J Physiol Heart Circ Physiol* 289: H2272–H2279, 2005.
19. **Liu J, Simpson DM, Allen R.** High spontaneous fluctuations in arterial blood pressure improves the assessment of cerebral autoregulation. *Physiol Meas* 26: 725–741, 2005.
20. **Mitsis G, Poulin MJ, Robbins PA, Marmarelis VZ.** Nonlinear modeling of the dynamic effects of arterial pressure and CO_2 variations on cerebral blood flow in healthy humans. *IEEE Trans Biomed Eng* 51: 1932–1943, 2004.
21. **Mitsis GD, Zhang R, Levine BD, Marmarelis VZ.** Cerebral hemodynamics during orthostatic stress assessed by nonlinear modeling. *J Appl Physiol* 101: 354–366, 2006.
22. **Moody M, Panerai RB, Eames PJ, Potter JF.** Cerebral and systemic hemodynamic changes during cognitive and motor activation paradigms. *Am J Physiol Regul Integr Comp Physiol* 288: R1581–R1588, 2005.
23. **Nakagawa K, Serrador JM, LaRose SL, Moslehi F, Lipsitz LA, Sorond FA.** Autoregulation in the posterior circulation is altered by the metabolic state of the visual cortex. *Stroke* 40: 2062–2067, 2009.
24. **Panerai RB.** Assessment of cerebral pressure autoregulation in humans: a review of measurement methods. *Physiol Meas* 19: 305–338, 1998.
25. **Panerai RB.** The critical closing pressure of the cerebral circulation. *Med Eng Phys* 25: 621–632, 2003.
26. **Panerai RB.** Transcranial Doppler for evaluation of cerebral autoregulation. *Clin Auton Res* 19: 197–211, 2009.
27. **Panerai RB, Carey BJ, Potter JF.** Short-term variability of cerebral blood flow velocity responses to arterial blood pressure transients. *Ultrasound Med Biol* 29: 31–38, 2003.
28. **Panerai RB, Deverson ST, Mahony P, Hayes P, Evans DH.** Effect of CO_2 on dynamic cerebral autoregulation measurement. *Physiol Meas* 20: 265–275, 1999.
29. **Panerai RB, Eames PJ, Potter JF.** Variability of time-domain indices of dynamic cerebral autoregulation. *Physiol Meas* 24: 367–381, 2003.
30. **Panerai RB, Moody M, Eames PJ, Potter JF.** Dynamic cerebral autoregulation during brain activation paradigms. *Am J Physiol Heart Circ Physiol* 289: H1202–H1208, 2005.
31. **Panerai RB, Rennie JM, Kelsall AWR, Evans DH.** Frequency-domain analysis of cerebral autoregulation from spontaneous fluctuations in arterial blood pressure. *Med Biol Eng Comput* 36: 315–322, 1998.
32. **Panerai RB, Sammons EL, Smith SM, Rathbone WE, Bentley S, Potter JF, Samani NJ.** Continuous estimates of dynamic cerebral autoregulation: influence of non-invasive arterial blood pressure parameters. *Physiol Meas* 29: 497–513, 2008.
33. **Panerai RB, Simpson DM, Deverson ST, Mahony P, Hayes P, Evans DH.** Multivariate dynamic analysis of cerebral blood flow regulation in humans. *IEEE Trans Biomed Eng* 47: 419–423, 2000.
34. **Paulson OB, Strandgaard S, Edvinson L.** Cerebral autoregulation. *Cerebrovasc Brain Metab Rev* 2: 161–192, 1990.
35. **Peng T, Rowley AB, Ainslie PN, Poulin MJ, Payne SJ.** Multivariate system identification for cerebral autoregulation. *Ann Biomed Eng* 36: 308–320, 2008.
36. **Poulin MJ, Liang PJ, Robbins PA.** Dynamics of the cerebral blood flow response to step changes in end-tidal P_{CO_2} and P_{O_2} in humans. *J Appl Physiol* 81: 1084–1095, 1996.
37. **Poulin MJ, Liang PJ, Robbins PA.** Fast and slow components of cerebral blood flow response to step decreases in end-tidal P_{CO_2} in humans. *J Appl Physiol* 85: 388–397, 1998.
38. **Rowley AB, Payne S, Tachtisdis I, Ebden MJ, Whiteley JP, Gavaghan DJ, Tarassenko L, Elwell CE, Delpy DT.** Synchronization between arterial blood pressure and cerebral oxyhaemoglobin concentration investigated by wavelet cross-correlation. *Physiol Meas* 28: 161–173, 2007.
39. **Serrador JM, Picot PA, Rutt BK, Shoemaker JK, Bondar RL.** MRI measures of middle cerebral artery diameter in conscious humans during simulated orthostasis. *Stroke* 31: 1672–1678, 2000.
40. **Simpson DM, Panerai RB, Evans DH, Garnham J, Naylor AR, Bell PRF.** Estimating normal and pathological dynamic responses in cerebral blood flow velocity to step changes in end-tidal P_{CO_2}. *Med Biol Eng Comput* 38: 535–539, 2000.
41. **Tiecks FP, Lam AM, Aaslid R, Newell DW.** Comparison of static and dynamic cerebral autoregulation measurements. *Stroke* 26: 1014–1019, 1995.
42. **Ursino M, Ter Minassian A, Lodi CA, Beydon L.** Cerebral hemodynamics during arterial and CO_2 pressure changes: in vivo prediction by a mathematical model. *Am J Physiol Heart Circ Physiol* 279: H2439–H2455, 2000.
43. **van Lieshout JJ, Wieling W, Karemaker JM, Secher NH.** Syncope, cerebral perfusion and oxygenation. *J Appl Physiol* 94: 833–848, 2003.
44. **Vern BA, Schuette WH, Leheta B, Juel VC, Radulovacki M.** Low-frequency oscillations of cortical oxidative metabolism in waking and sleep. *J Cereb Blood Flow Metab* 8: 215–226, 1988.
45. **Widder B, Kleiser B, Krapf H.** Course of cerebrovascular reactivity in patients with carotid artery occlusions. *Stroke* 25: 1963–1967, 1994.
46. **Zhang R, Zuckerman JH, Giller CA, Levine BD.** Transfer function analysis of dynamic cerebral autoregulation in humans. *Am J Physiol Heart Circ Physiol* 274: H233–H241, 1998.
47. **Zou R, Cupples WA, Yip KP, Holstein-Rathlou NH, Chon KH.** Time-varying properties of renal autoregulatory mechanisms. *IEEE Trans Biomed Eng* 49: 1112–1120, 2002.